ACS OMEGA

Article

http://pubs.acs.org/journal/acsodf

Fabrication of Core−Shell-Structured Organic−Inorganic Hybrid Nanocatalyst for the Expedient Synthesis of Polysubstituted Oxazoles via Tandem Oxidative Cyclization Pathway

Sriparna Dutta, Shivani Sharma, Aditi Sharma, and Rakesh K. Sharma*

Green Chemistry Network Centre and Department of Chemistry, University of Delhi, New Delhi 110007, India

Supporting Information

ABSTRACT: The quest for designing efficient heterogeneous catalytic systems for tandem oxidative cyclization reactions has provided a great impetus to research efforts, as it enables the step-economic construction of complex heterocyclic molecules as well as confers the benefits of a facile catalytic recovery. In the present study, we disclose a new core−shell-structured organic−inorganic hybrid copper nanocatalyst fabricated via the covalent grafting of 2,2′-dipyridyl ketone ligand on amine-functionalized silica-encapsulated magnetite nanoparticles, followed by its metallation with cupric acetate for the tandem oxidative cyclization of amines and β-ketoesters, leading to the production of biologically active polysubstituted oxazole moieties. This programmed catalytic protocol proceeds via the formation of intermolecular C−C and C−N bonds by single-step synthesis and accommodates a broad combination of reaction coupling partners.

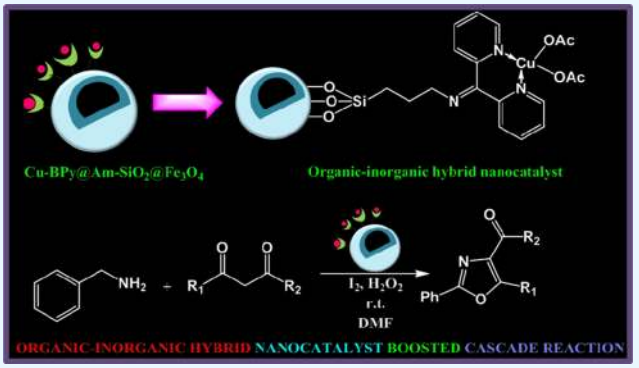

1. INTRODUCTION

Synthetic organic chemistry has reached a crucial point in which new paradigms are needed to achieve the challenging goals of step economy and waste reduction. Tandem reactions, often called cascade reactions that are capable of smartly combining different organocatalytic reaction steps in a single-pot synthesis, have emerged as one of the most powerful and practical tools to construct complex heterocyclic architectures for multifaceted intents.[1−6] In fact, these reactions have proliferated in the area of total organic synthesis ever since the publication of the pioneering work of Robinson in 1917 on the seminal synthesis of tropinone.[7] The main driving force of the huge synthetic efforts is the undeniable benefits of high atom economy and reduced waste generation, which cause such reactions to fall under the banner of green chemistry.[8] Besides enabling the economical and environmentally friendly synthesis of targeted molecules of considerable structural and stereochemical complexity, the cascade processes expand our repertoire of reactions and strategies by allowing the use of synthetically enabling intermediates that may or may not be practical or possible to isolate.[9] Indeed, it is the enduring efficiency and overall esthetic appeal of these processes that have prompted chemists to explore novel reaction cascades for the synthesis of complex polycyclic ring skeletons, which serve as important scaffolds of natural products with important bioactivities. In this direction, the recent attempts to obtain the exceedingly significant biologically active polysubstituted oxazole moieties using the copper-catalyzed tandem oxidative cyclization (TOC) pathway are worth applauding.[10−15] Although this strategy presents a convincible methodological refinement over the classical procedures in terms of the drastic enhancement in atom economy and reaction conditions, yet the exploitation of homogeneous metal salt as the catalyst renders its commercial utility rather bleak because of the associated problems of separation and recovery. In view of these limitations, the search for a sustainable heterogeneous catalyst that can provide a ready access to the target oxazole moieties remains an important yet elusive objective for engineering oxidative cyclization reactions. So far, no such capable heterogeneous catalyst has been created that can be applied for this transformation successfully, which is precisely the reason that ignited the spark of interest within us.

Modern state of the art of catalysis science and research reveals that the introduction of novel nanotechnologies has enabled the generation of solid-supported heterogeneous nanoscale catalysts, which are effective tools for controlling chemical reactivity as well as conferring the synergistic benefits of facile recovery.[16−26] By collectively integrating the key advantages of homogeneous as well as heterogeneous catalysts, they offer great prospects of meeting the sustainability criteria consistent with the goals of green chemistry. However, the selection of an appropriate support material is extremely crucial in designing such potent catalysts, as the spatial structure of the support plays an important role in holding the active site

Received: March 30, 2017
Accepted: June 5, 2017
Published: June 19, 2017

DOI: 10.1021/acsomega.7b00382
ACS Omega 2017, 2, 2778−2791

Scheme 1. Synthetic Pathway for Obtaining Cu-BPy@Am-SiO_2@Fe_3O_4 Core−Shell Nanocatalyst

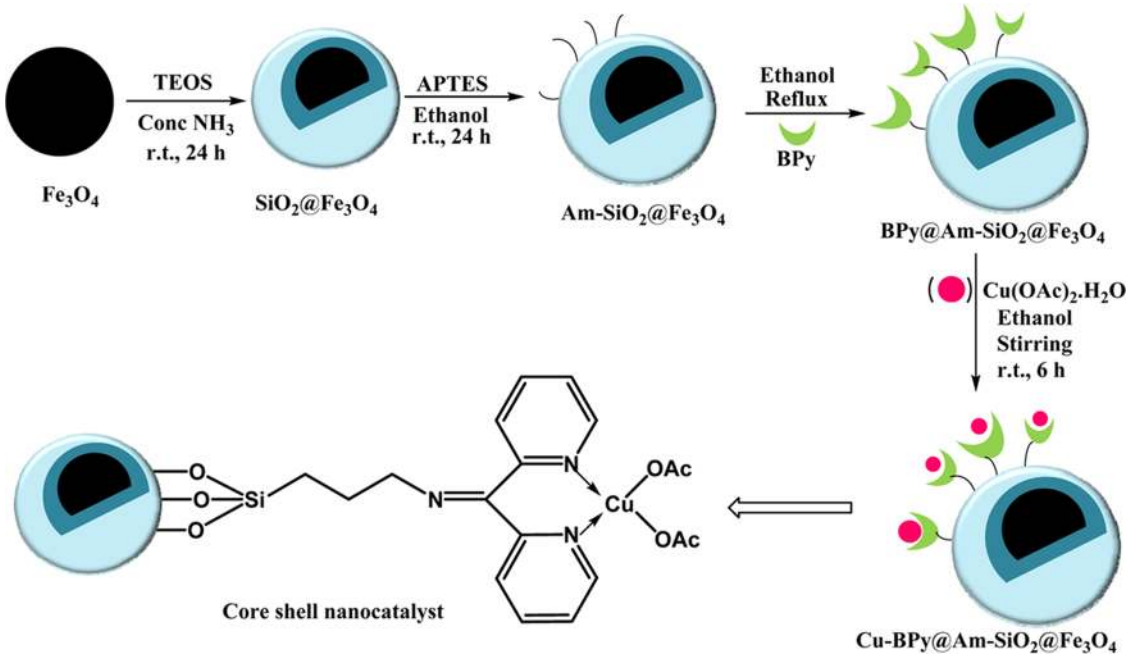

through strong coordination during the catalysis. Among a multitude of solid matrices explored to date,[27−39] core−shell-structured silica-encapsulated magnetic nanoparticles have shown their unrivaled power owing to the combined benefits of a superparamagnetic core material that permits/endows easy catalyst separation (using an external magnet) and a surrounding shell that imparts durability to the synthesized catalyst by protecting the core from agglomerating, sintering, or undergoing oxidation.[40−53] In addition, the shell provides the opportunity to tune the structure and consequently the performance of the catalyst by allowing the immobilization of a diverse array of reagents, such as linkers and functionalized ligands. Thus, it is not surprising that the field of "design and synthesis of magnetically recyclable core−shell nanocatalysts" is experiencing an explosive growth, with many exciting developments in the new millennium.

The recent fast-growing research on such potential nanomaterials inspired us to come up with new silica-based magnetically retrievable core−shell nanocatalytic systems that proved their efficiency in different organic transformations, such as C−H activation of formamides and reductive amination of ketones.[54,55] Impressed by the catalytic efficacy of such materials and in conjunction with our ongoing research work in the design and development of sustainable nanocatalysts,[56−66] we decided to exploit the catalytic properties of the core−shell support material, ligand, linker, and transition metal. Using a covalent immobilization strategy, we fabricated a magnetic silica-based copper nanocatalyst, which was characterized well by advanced combined electron microscopy (high-resolution transmission electron microscopy (HRTEM), scanning electron microscopy (SEM)) and spectroscopic (Fourier transform infrared (FTIR), energy-dispersive X-ray (EDX), energy-dispersive X-ray fluorescence (EDXRF), wide-angle X-ray diffraction (WAXRD), inductively coupled plasma (ICP)) techniques. This novel material was then used in the tandem oxidative cyclization reaction to obtain the desired/significant polysubstituted oxazole products under mild experimental conditions. Much to our satisfaction, we found that this new heterogeneous copper catalyst not only facilitated the formation of the desired products with good to excellent conversion but also enhanced the economic viability of the protocol greatly because: (i) this new procedure replaced *tert*-butyl hydroperoxide (TBHP) with H_2O_2, which is a greener oxidant and (ii) for the very first time, we employed a heterogeneous catalyst for this process that could be recovered easily by magnetic attraction and further reused for several test cycles. Therefore, in this study, we report the first example of a heterogeneously catalyzed protocol for the TOC approach toward the synthesis of polysubstituted oxazoles that opens up a new and promising insight into the course of rational design, synthesis, and applications of core−shell magnetic nanoparticle complexes for such reactions.

2. RESULTS AND DISCUSSION

The catalyst was prepared in a step-by-step manner, beginning from the synthesis of magnetite nanoparticles (Fe_3O_4), as shown in Scheme 1.

For obtaining Fe_3O_4 nanoparticles, a previously reported coprecipitation approach was implemented.[67] This was followed by silica encapsulation of the nanoparticles using the modified sol−gel process in the presence of tetraethyl orthosilicate (TEOS) as the silica precursor.[68] In the next step, silica-coated magnetite nanoparticles were functionalized using 3-aminopropyltriethoxysilane (APTES), wherein the NH_2 linker was coupled to its surface.[69] Thereafter, ligand 2,2′-bipyridyl ketone (BPy) was covalently immobilized on the surface of the functionalized nanoparticles.[70] In the last step, ligand-grafted nanoparticles were metallated with cupric acetate for fabricating the nanocatalyst. The synthesized nanocomposites were thereafter characterized methodically using different physicochemical techniques, including TEM, SEM, EDX spectroscopy, EDXRF spectroscopy, FTIR spectroscopy, WAXRD, ICP, and vibrating sample magnetometer (VSM) analysis.

2.1. Catalyst Characterization. WAXRD is an effective technique that can shed light on the presence of core−shell

DOI: 10.1021/acsomega.7b00382
ACS Omega 2017, 2, 2778−2791

structures in the synthesized nanoparticles. Thus, this technique was utilized for investigating the crystalline phases of the magnetite nanoparticles before and after silica coating (Figure 1). The WAXRD patterns of both Fe_3O_4 and SiO_2@Fe_3O_4

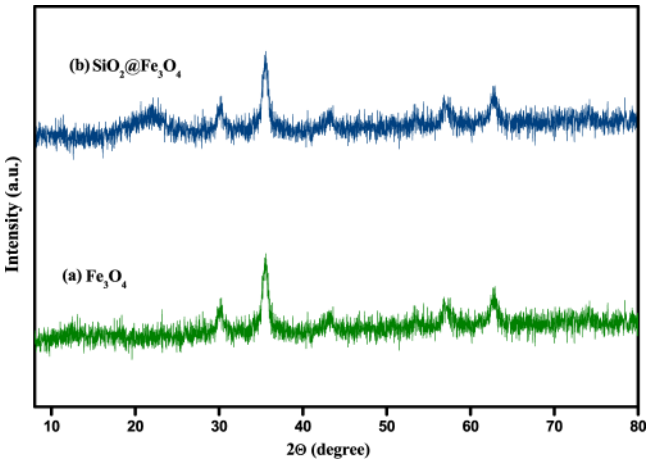

Figure 1. WAXRD spectrum of (a) Fe_3O_4 and (b) SiO_2@Fe_3O_4 nanoparticles.

nanoparticles displayed six characteristic diffraction peaks at specific 2θ values, corresponding to the inverse spinel structure of magnetite well matched by the Joint Committee on Powder Diffraction Standards (JCPDS) data (JCPDS card no.: 19-629). This result clearly signified that the magnetic component is well retained in the prepared nanocomposites even after the silica encapsulation process. However, in contrast to that of pure Fe_3O_4, the WAXRD spectrum of SiO_2@Fe_3O_4 showed the presence of a broad hump around $2\theta = 20–23°$, which could be attributed to the silica shell surrounding the core material; thus, the emergence of this new peak certified the successful encapsulation of bare magnetite nanoparticles.[68] Furthermore, we evaluated the crystallite size of the nanoparticles by picking the peak of highest intensity in the WAXRD spectrum of Fe_3O_4 and applying the Debye–Scherrer formula to it (i.e., $D_{hkl} = k\lambda l/\beta \cos\theta$, where D is the size of the axis parallel to the hkl plane, k is a constant with a typical value of 0.89 for spherical particles, β is the full width at half-maxima in radians, and θ is Bragg's angle in degrees). The average size of the nanoparticles was evaluated to be 11.9 nm according to the above equation.

TEM images were acquired to gain an insight into the morphological characteristics of the nanoparticles. Observation by this analysis revealed that Fe_3O_4 nanoparticles possess a roughly spherical morphology with an average diameter of 8–12 nm (Figure 2). The selected-area electron diffraction (SAED) pattern recorded on a single particle showed the presence of white spotty diffraction rings assignable to the [220], [311], [400], [422], [511], and [440] planes of the cubic inverse spinel structure of magnetite. The appearance of these distinct diffraction rings also confirmed the polycrystalline nature of the nanoparticles. For a detailed structural analysis, HRTEM image of the pristine magnetite nanoparticles was captured. This image reflected two-dimensional lattice fringes that could be indexed to the (220) plane of pure magnetite with an interplanar separation value of 0.25 nm. The core–shell morphology of the silica-coated nanoparticles was well supported by the representative TEM image of SiO_2@Fe_3O_4. Distinctively, it could be seen that the black inner core material is well embedded within the light gray silica shell. The thickness of this shell was measured to be approximately 10 nm. Further, the TEM image of final catalyst was also provided, which shows that the metal complex is uniformly embedded over the core–shell surface and the particles exhibit a spherical morphology very similar to that of the native Fe_3O_4 nanoparticles (Figure S1).

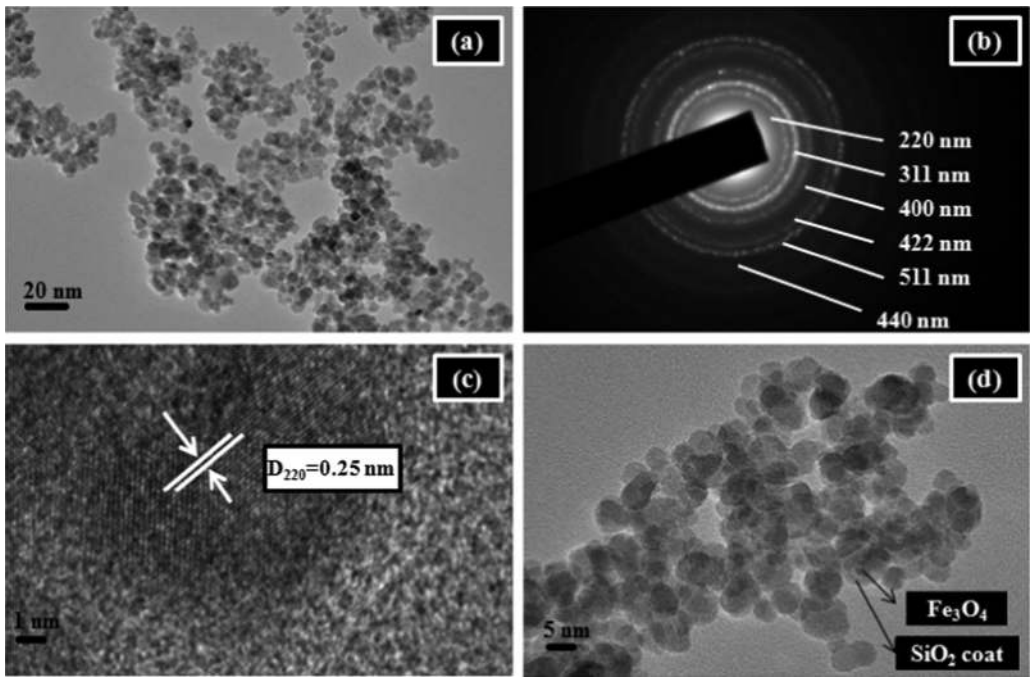

Figure 2. (a) TEM image of synthesized Fe_3O_4 nanoparticles, (b) SAED pattern of Fe_3O_4, (c) HRTEM image of the single nanocrystal entity with lattice fringe, and (d) TEM image of SiO_2@Fe_3O_4.

DOI: 10.1021/acsomega.7b00382
ACS Omega 2017, 2, 2778–2791

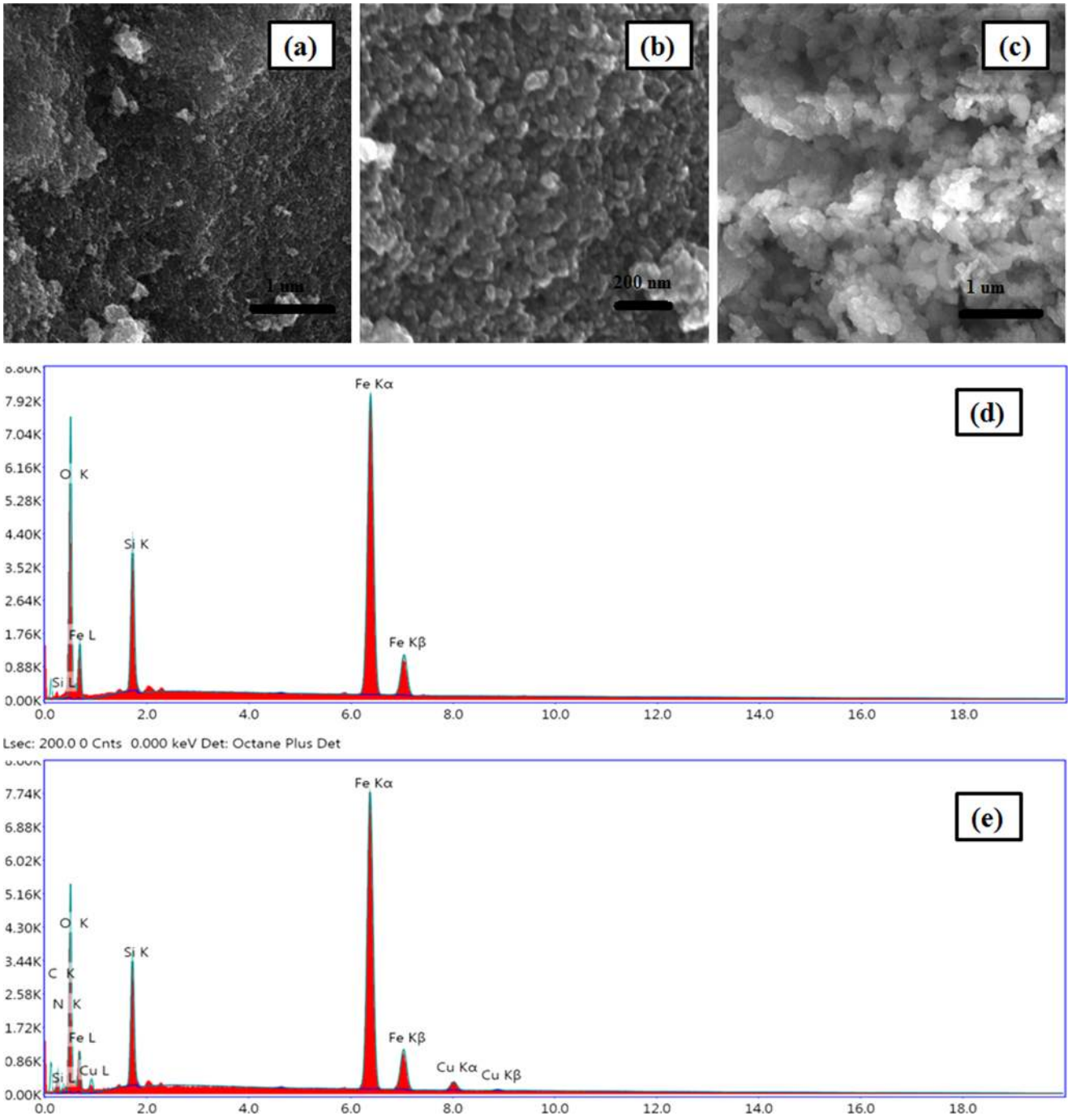

Figure 3. FESEM images of (a) Fe_3O_4, (b) SiO_2@Fe_3O_4, and (c) Cu-BPy@Am-SiO_2@Fe_3O_4 and EDX spectra of (d) SiO_2@Fe_3O_4 and (e) Cu-BPy@Am-SiO_2@Fe_3O_4.

Surface morphology of the nanoparticles was characterized by the highly sophisticated field emission scanning electron microscopy (FESEM) technique. Typical FESEM images of Fe_3O_4, SiO_2@Fe_3O_4, and Cu-BPy@Am-SiO_2@Fe_3O_4 are depicted in Figure 3. A closer look into the obtained images divulged that the spherical morphology of the synthesized nanoparticles was intact even after the silica coating and successive catalyst synthesis steps. However, a noticeable surface roughening had occurred on moving from Fe_3O_4 to SiO_2@Fe_3O_4 to the final nanocatalyst. Such a distinct surface-roughening phenomenon could be attributed to the deposition of various surface-modifying species, such as silica, amine group, ligand, and metal, around the core material. Also, appreciably, no separate silica aggregates were observed that ruled out the possibility of precipitation of primary silica nanoparticles. Further, information regarding the chemical composition of the core−shell nanocomposites (particularly, SiO_2@Fe_3O_4 and Cu-BPy@Am-SiO_2@Fe_3O_4) was gained with the help of EDX spectroscopy. The presence of Fe, Si, and O in the EDX survey spectra of the silica-coated magnetite nanoparticles confirmed the existence of the silane shell around the superparamagnetic core. In addition to these three vital elements, distinct peaks of nitrogen, oxygen, and copper substantiated the successful immobilization of functionalizing

DOI: 10.1021/acsomega.7b00382
ACS Omega 2017, 2, 2778−2791

agent, ligand, and metal on the surface of the silica-coated magnetite nanosupport, thus certifying the final structure of the nanocatalyst. The support for the presence of copper in the fabricated catalyst was further provided by the EDXRF technique (the well-resolved peak of copper in the EDXRF spectrum of Cu-BPy@Am-SiO_2@Fe_3O_4 shown in Figure S2 clearly authenticated the synthesis of the catalyst). Next, the amount of copper present in the catalyst was determined through the ICP technique performed by first carrying out the sample digestion in aqua regia using microwave irradiation for 10 min at 400 W, followed by adjusting the volume of the filtrate to 100 mL using double-deionized water, and 0.1542 mmol g^{-1} of copper was quantified using calibration curve in duplicate for each sample.

For the stepwise characterization of the synthesized nanocomposites, FTIR spectroscopic analysis was performed under the scanning range of 4000−400 cm^{-1} using KBr pellets. The appearance of specific functional groups at every stage of catalyst preparation helped in authenticating the structures of the parent nanocomposites and the final catalyst. The FTIR spectra of the pristine Fe_3O_4, SiO_2@Fe_3O_4, Am-SiO_2@Fe_3O_4, BPy@Am-SiO_2@Fe_3O_4, and Cu-BPy@Am-SiO_2@Fe_3O_4 nanoparticles are shown in Figure 4. The emergence of a strong and

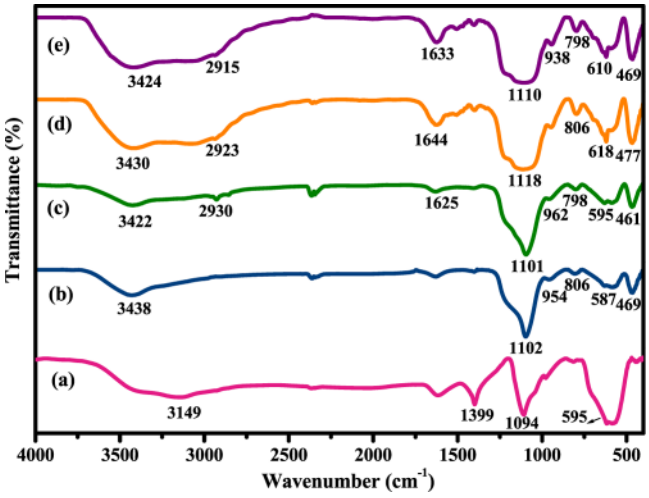

Figure 4. FTIR spectra of (a) Fe_3O_4, (b) SiO_2@Fe_3O_4, (c) Am-SiO_2@Fe_3O_4, (d) BPy@Am-SiO_2@Fe_3O_4, and (e) Cu-BPy@Am-SiO_2@Fe_3O_4.

intense absorption band at 589 cm^{-1} attributable to the characteristic Fe−O stretching vibrations and another broad band centred around 3124 cm^{-1} assignable to the deforming vibrations of adsorbed water in the FTIR spectrum of Fe_3O_4 nanoparticles provided a concrete proof for the structure of the magnetite core.[71] On moving toward silica-coated magnetite nanoparticles (SiO_2@Fe_3O_4), an obvious reduction in the intensity of the Fe−O and OH stretching bands was observed, which could be attributed to the introduction of the silane moiety (amorphous SiO_2). In addition, three new peaks appearing at 806, 954, and 1102 cm^{-1} could be assigned to the Si−O−Si symmetric, Si−O symmetric, and Si−O−Si asymmetric stretching modes of the silica framework, respectively.[72]

These results validated the successful encapsulation of the core material by the silane shell. The evidence for the functionalization of the silica-coated nanosupport was further acquired from the occurrence of two new absorption peaks at 2930 and 1625 cm^{-1} belonging to the CH_2 and NH_2 groups of the aminopropyl moiety of Am-SiO_2@Fe_3O_4 nanoparticles, respectively. The ligand-grafted nanoparticles on the other hand, besides displaying all of the distinct peaks of amine-functionalized nanoparticles, showed a strong band at 1644 cm^{-1} because of the C═N stretching vibration of the ligand (BPy). After metallation, this band shifted to a lower value (i.e., 1633 cm^{-1}), which suggested the formation of a bond between the copper and the ligand. In our previous studies, we observed similar band shifts in the IR spectrum. These results collectively signified that the copper species are effectively immobilized on modified silica-coated magnetite nanoparticles as a BPy−copper complex.

After carrying out a detailed morphological and compositional analysis, our focus shifted toward exploring the magnetic properties of the catalyst (the most important property that accounts for the facile recovery of the catalyst). A VSM was employed for this purpose, and a comparative analogy of the magnetic hysteresis measurements of the prepared core−shell nanomaterials (SiO_2@Fe_3O_4 and Cu-BPy@Am-SiO_2@Fe_3O_4) and the uncoated magnetite (Fe_3O_4) was made in an external field sweeping between −20 000 and 20 000 Oe at room temperature (r.t.) (Figure 5). The registered magnetization

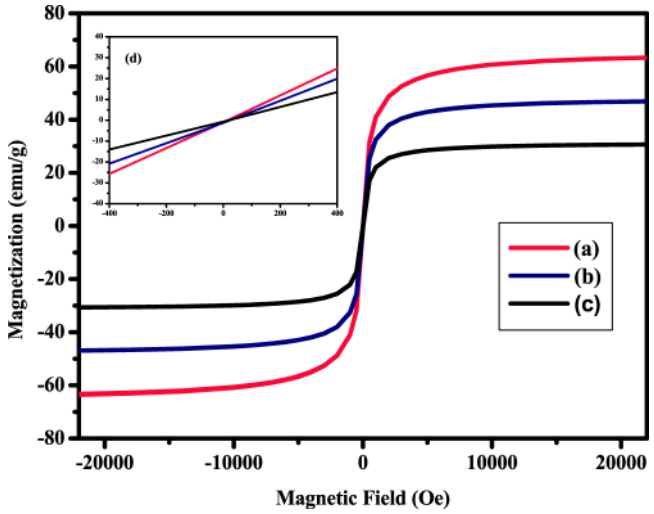

Figure 5. Magnetization curves obtained by VSM at r.t. for (a) Fe_3O_4, (b) SiO_2@Fe_3O_4, and (c) Cu-BPy@Am-SiO_2@Fe_3O_4; (d) enlarged image near the coercive field.

curves reflected the superparamagnetic nature of the nanocomposites because of the absence of the hysteresis phenomenon. To further substantiate this typical feature of superparamagnetism, a narrower magnetization range was selected and plotted (shown in the inset of Figure 5). Quite apparent from the plot, both magnetization and demagnetization curves passed through the origin, showing negligible coercivity (Hc, Oe) and remanence (Mr, emu g^{-1}). These results confirmed the superparamagnetic properties of the synthesized nanoparticles. Further, the saturation magnetization, extracted from the corresponding VSM curves, for the uncoated magnetite sample was found to be 63.5 emu g^{-1}, whereas this value decreased to 46.9 and 30.6 emu g^{-1} for the coated samples. This gradual decrease in the magnetization value of the core−shell nanomaterials (SiO_2@Fe_3O_4 and Cu-BPy@Am-SiO_2@Fe_3O_4) could be attributed to the incorpo-

DOI: 10.1021/acsomega.7b00382
ACS Omega 2017, 2, 2778−2791

ration of the nonmagnetic silica shell around the core, which decreased the magnetic coupling interactions between the neighboring magnetite nanoparticles.[73] A possible mechanism that could be proposed for this reduction was the disappearance of magnetic moments of Fe due to the surface functionalization of these ions with silica to form Fe−O−Si chemical bonds. However, it is worth mentioning here that despite the lowering of the M_s values, the final nanocatalyst showed ease of separation from the reaction mixture.

2.2. Activity of the Obtained Nanocatalyst in the Synthesis of Polysubstituted Oxazoles Using the Tandem Cyclization Approach. After structural verification of the fabricated core−shell-structured copper nanocatalyst, we explored its applicability in the tandem oxidative cyclization of 1,3-dicarbonyl compounds and amines for obtaining industrially significant oxazoles. To get an insight into the optimum catalytic conditions, methylacetoacetate and benzylamine were chosen as the model substrates. Consequently, we screened a number of solvents, oxidants, and additives for establishing the most compatible reaction conditions. Further, with the same objective in mind, we investigated the effects of crucial experimental variables, such as temperature, time, and substrate molar ratio, on this reaction.

In the initial phase of our study, we performed a controlled experiment, wherein a 1:2 mixture of the test substrates (i.e., 1 equiv methylacetoacete and 2 equiv benzylamine) was reacted at r.t. under catalyst-free conditions. Almost negligible conversion occurred in this case despite continuing the reaction for a prolonged duration, which underscored the significance of a catalyst in tandem oxidative process (Table 1).

Table 1. Effects of Different Catalysts on the Tandem Oxidative Cyclization of Amines and 1,3-Dicarbonyls[a]

entry	catalyst	conv. %[b]	TON[c]	TOF[d]
1	no catalyst	5		
2	Fe_3O_4	10	39	13
3	SiO_2@Fe_3O_4	12	47	16
4	Am-SiO_2@Fe_3O_4	8	31	10
5	Cu@Am-SiO_2-Fe_3O_4	45	177	59
6	Cu-BPy@Am-SiO_2@Fe_3O_4	100	393	131

[a]Reaction conditions: methylacetoacetate (1 mmol), benzylamine (2 mmol), catalyst (30 mg), H_2O_2 (3 equiv), I_2 (1.2 equiv), dimethylformamide (DMF, 3 mL), r.t., 3 h. [b]Conversion percentages were determined via gas chromatography−mass spectrometry (GC−MS). [c]TON is the number of moles of product per mole of catalyst. [d]TOF = TON/h.

Next, we employed different catalysts and checked their efficacy in affording the target product. As anticipated, the use of only Fe_3O_4, SiO_2@Fe_3O_4, and Am-SiO_2@Fe_3O_4 resulted in a very poor reaction conversion (Table 1, entries 2−4). On the other hand, when different copper-based sources were used, the desired tandem product was obtained with a good conversion. Among all of the tested catalytic sources, the heterogeneous copper nanocatalyst undeniably exhibited the highest conversion percentage.

We also evaluated the effect of catalyst concentration on the model reaction. To understand how this parameter affected the reaction profile, we conducted six experiments, in which we simply increased the amount of catalyst from 5 to 30 mg. The results revealed that an increase in the amount of catalyst leads to an almost exponential rise in the conversion percentage, which was primarily due to the subsequent increase in the active sites of the nanoscale heterogeneous catalyst (Figure 6). The amount of catalyst was optimized to 30 mg, as it was sufficient enough to result in maximum conversion.

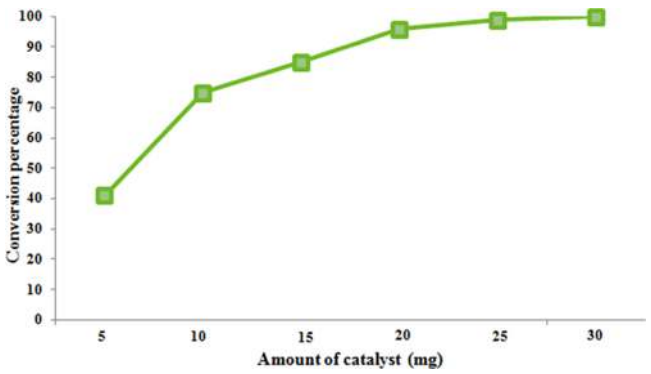

Figure 6. Effect of the amount of catalyst on the tandem oxidative cyclization of amines and 1,3-dicarbonyls [reaction conditions: methylacetoacetate (1 mmol), benzylamine (2 mmol), Cu-BPy@Am-SiO_2@Fe_3O_4 catalyst (x mg), H_2O_2 (3 equiv), I_2 (1.2 equiv), DMF (3 mL), r.t., 3 h].

Subsequently, we focused our attention toward optimizing the solvent. Surprisingly, we found that the polarity of the solvents played a critical role in determining the efficiency of the cascade process. However, nonpolar solvents like toluene, acetonitrile, chloroform, and tetrahydrofuran resulted in a poor conversion of reactants used: a drastic increment was observed on switching the solvent from nonpolar to polar (Figure 7). DMF proved its prowess in this reaction, as the best results were achieved in this case.

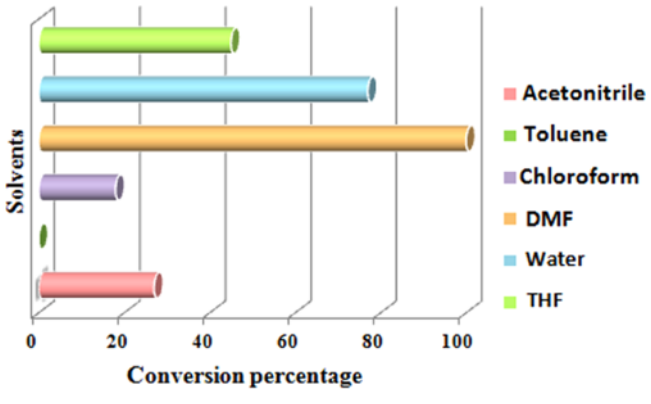

Figure 7. Effects of solvents on the tandem oxidative cyclization of amines and 1,3-dicarbonyls [reaction conditions: methylacetoacetate (1 mmol), benzylamine (2 mmol), Cu-BPy@Am-SiO_2@Fe_3O_4 catalyst (30 mg), H_2O_2 (3 equiv), I_2 (1.2 equiv), solvent (3 mL), r.t., 3 h].

Success of oxidative C(sp^3)−H cascade reactions is largely dependent on the efficiency of the employed oxidant. Thus, in developing such protocols, it is very important to select the appropriate oxidant, as a number of factors, such as versatility, expense, and environmental impact, need to be addressed. Keeping this in mind, we moved toward screening the most crucial parameter of the reaction, that is, oxidant. For doing so, we investigated a wide array of oxidants. The results of this screening experiment rather surprised us. Unlike in most of the previously established protocols,[11,12] where TBHP had proved

DOI: 10.1021/acsomega.7b00382
ACS Omega 2017, 2, 2778−2791

to be an oxidant of choice, we found that in our heterogeneously catalyzed protocol a greener oxidant, hydrogen peroxide, which generates water as the sole byproduct, performed much better, as 100% conversion was accomplished in this case. Oxidant concentration also significantly affected the reaction conversion, which is apparent from the results shown in Figure 8. We began the first set of experiment with 0.5 equiv

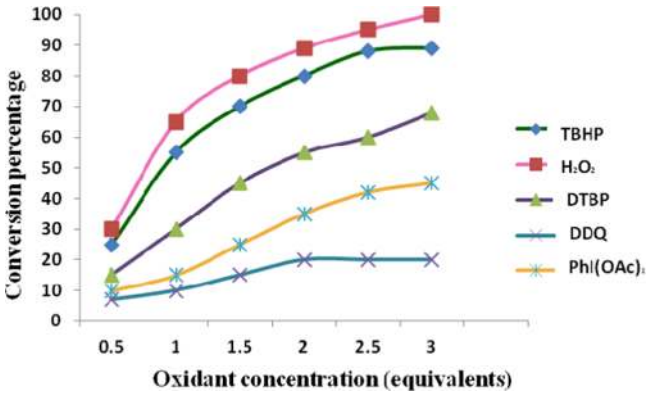

Figure 8. Effect of oxidant and oxidant concentration on tandem oxidative cyclization of amines and 1,3-dicarbonyls [reaction conditions: methylacetoacetate (1 mmol), benzylamine (2 mmol), Cu-BPy@Am-SiO_2@Fe_3O_4 catalyst (30 mg), oxidant (x equiv), I_2 (1.2 equiv), DMF (3 mL), r.t., 3 h].

of oxidant and found that only 30% conversion could be achieved in this case. To accomplish better results, we increased the oxidant concentration from 0.5 to 3 equiv. Ecstatically, a drastic improvement in the results was observed as the conversion increased rapidly on increasing oxidant equivalents and the best results were obtained when 3 equiv of oxidant (H_2O_2) were used.

Thereafter, to improve the reaction efficiency, we introduced additives into the reaction system. A thorough literature survey provided us a clue that iodine-based compounds could enhance the overall conversion of the concerned reaction, as they show impressive catalytic activity in the formation of new C−C, C−O, and C−N bonds in organic compounds because of their electrophilic properties.[74,75] Hence, different iodine-based sources, such as potassium iodide (KI), tetrabutylammonium iodide (TBAI), N-Iodosuccinimide (NIS), and iodine (I_2), were investigated for this tandem oxidative cyclization reaction (Table S1). To our delight, we found that molecular I_2, which has received considerable attention[76−78] in recent years as an inexpensive, environmentally friendly, and readily available reagent to effect iodocyclization and cyclodehydroiodination reactions, worked quite well as an additive in this reaction, as it resulted in the maximum conversion of the employed reactants. The optimization studies showed that the addition of I_2 was crucial for cyclizing the model substrates.

Finally, we modulated the reaction time and temperature and examined the effects of these two crucial parameters on the synthesis of oxazoles. The conversion percentages were plotted as a function of time and temperature, and the results are shown in Figure 9.

It was noted that although an increase in temperature incurred lower reaction conversion, an increase in time period had a positive impact on the reaction conversion. Notably, r.t. (25 °C) and a time period of 3 h best suited the catalysis of this

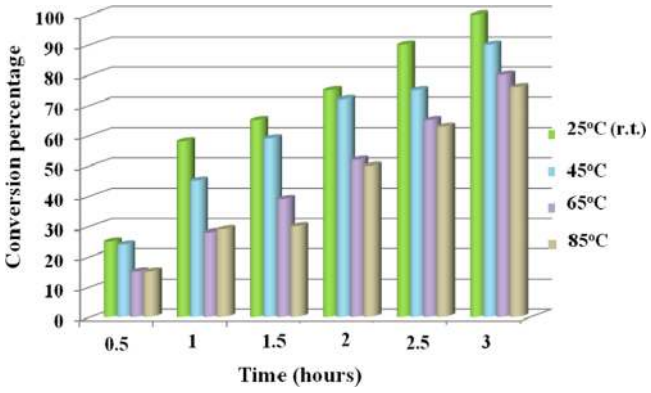

Figure 9. Effects of time and temperature on the tandem oxidative cyclization of amines and 1,3-dicarbonyls [reaction conditions: methylacetoacetate (1 mmol), benzylamine (2 mmol), Cu-BPy@Am-SiO_2@Fe_3O_4 catalyst (30 mg), H_2O_2 (3 equiv), I_2 (1.2 equiv), and DMF (3 mL)].

transformation and thus the rest of the catalytic experiments were performed under similar reaction conditions.

Under optimal oxidative conditions, we set out to probe the viability of this envisioned sequential catalytic protocol. For doing so, first we investigated the scope of substituted β-ketoesters bearing either alkyl or aromatic functional groups by reacting them with benzylamine under the established reaction conditions. The results are shown in Scheme 2. In general, we found that the corresponding oxazole products could be obtained with a good conversion percentage and a high turnover number. However, in case of bulky substituents, there was a slight decrease in the conversion, which could be attributed to the steric effect (Scheme 2, **3c** and **3f**). Next, we switched over to β-diketone and again found a profound decrease in the conversion, the reason for which remained unclear (Scheme 2, **3g**).

To further explore the substrate scope, we evaluated the scope of benzylamine derivatives bearing either electron-donating or electron-withdrawing group (Scheme 3).

Surprisingly and quite unexpectedly, benzylamines possessing electron-donating substituents on the aromatic ring (Scheme 3, **3h**, **3k**, and **3m**) showed better reactivity, that is, higher conversion percentage and turnover number, compared to those with electron-withdrawing substituents. Further, to demonstrate the synthetic utility of this protocol, we scaled up the model reaction to 50 mmol (Scheme S1). We were ecstatic to find that the conversion reached the same level as when it was performed on a small scale, which clearly illustrated the large-scale industrial applicability of this reaction.

2.3. Mechanism. To gain an insight into the reaction mechanism, a few control experiments were performed (Scheme 4), whose results revealed that the use of iodine, Cu-BPy@Am-SiO_2@Fe_3O_4 catalyst, and oxidant is essential for the full conversion of the reaction. Henceforth, on the basis of control experiments and previous studies,[11] a plausible reaction mechanism was proposed for the tandem oxidative cyclization protocol (Scheme 5). The first step involves the interaction between HOI (resulting from the reaction between I_2 and H_2O_2) and enol tautomer **2b** of the test substrate methylacetoacetate (**2a**), which leads to the formation of compound **4**. In the next step, nucleophilic attack of the NH_2 group of the benzylamine on the copper-coordinated iodo

DOI: 10.1021/acsomega.7b00382
ACS Omega 2017, 2, 2778−2791

Scheme 2. Substrate Scope for the Reaction of 1,3-dicarbonyls with Benzylamines[a–c]

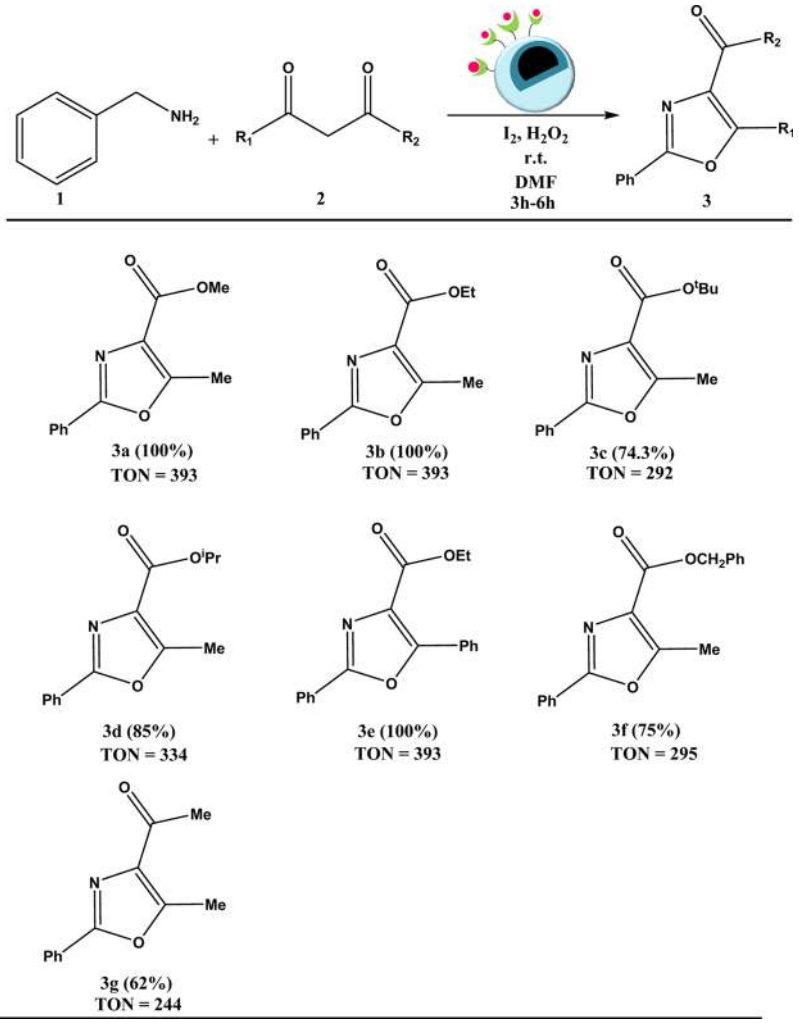

[a]Reaction conditions: 1,3-dicarbonyl (1 mmol), benzylamine (2 mmol), Cu-BPy@Am-SiO_2@Fe_3O_4 (30 mg), H_2O_2 (3 equiv), I_2 (1.2 equiv), DMF (3 mL), r.t. [b]Conversion percentages determined *via* GC-MS have been given in parentheses. [c]TON is the number of moles of the product per mole of the catalyst.

complex (**5**) generates compound **6**, which is facilitated by the removal of HI.

Compound **6** so generated undergoes oxidation in the presence of H_2O_2 to form compound **7**, which, in the presence of solid-supported copper catalyst, undergoes an intramolecular cyclization, giving intermediate **9** in a tandem process. Finally, oxidation of **9** affords the desired oxazole product (**3**).

2.4. Catalytic Activity Tests. *2.4.1. Heterogeneity Test.* To verify that the observed catalysis was due to the synthesized magnetite-supported copper nanocatalyst and not due to any leached metallic species, we carried out a standard leaching experiment using the hot filtration method reported in the literature.[79] During this test, the solid catalyst was removed from the reaction via magnetic forces at about half the reaction time and the reaction conversion was determined by GC–MS to be 62%. The resulting reaction mixture was subjected to further stirring for a prolonged duration to rule out any ambiguity due to shorter duration, and the reaction progress was monitored continually using GC–MS. No increase in the conversion percentage even after extended times proved the true heterogeneous nature of the catalyst by excluding the possibility of leaching of the active catalytic complex from the support. To further support this observation, ICP analysis of the supernatant was conducted. Much to our delight, we found that the copper content was less than the detection limits. Thereafter, using this exactly small amount of copper, independent homogeneous reactions were performed. No formation of the desired product occurred, which meant no homogeneous catalysis was involved. Also, UV–visible spectrum of the supernatant was obtained and the results were studied carefully. No peak of copper in this spectrum showed that the copper–BPy complex remained tightly anchored to the silica-coated magnetite support, indicating the stability of our synthesized catalyst.

2.4.2. Recyclability Test. For developing an efficient green system, "ready isolation and convenient recycling and reuse of catalyst" are highly desirable from the viewpoint of large-scale industrial applicability. Thus, in addition to the heterogeneity test, we checked the reusability of the synthesized catalyst. To do so, we carried out repeated runs of the model reaction using fresh reactants every time but on the same batch of the catalyst. The results of these experiments are shown in Figure 10. To regenerate the catalyst, after each run, it was separated by means of external magnetic attraction, washed several times

DOI: 10.1021/acsomega.7b00382
ACS Omega 2017, 2, 2778–2791

Scheme 3. Substrate Scope for the Reaction of Substituted Benzylamines with 1,3-dicarbonyls[a–c]

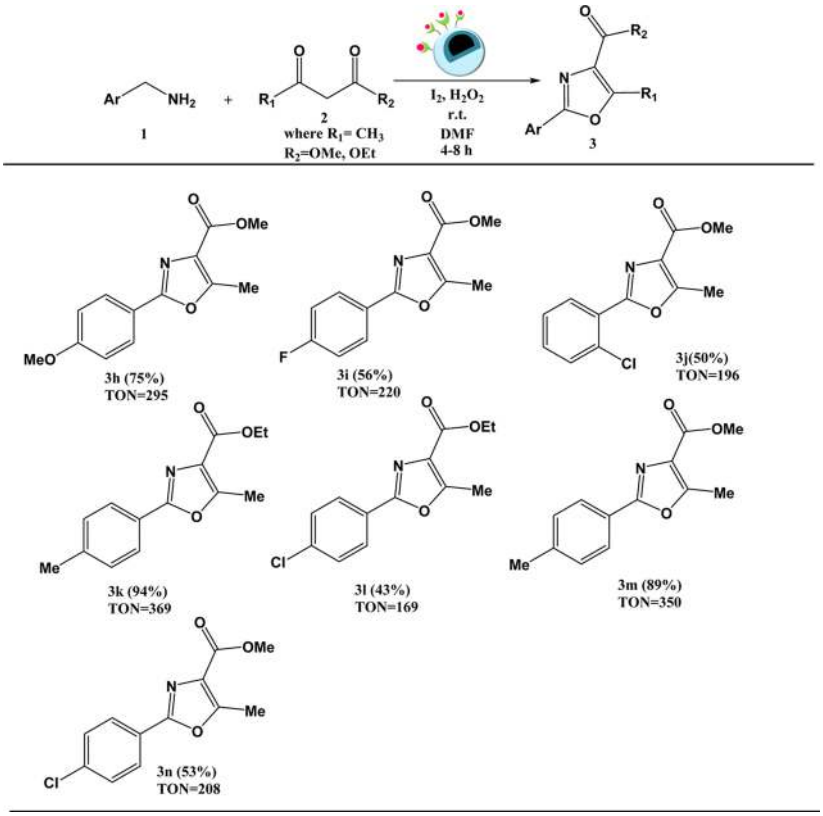

[a]Reaction conditions: benzylamine derivatives (2 mmol), 1,3-dicarbonyl (1 mmol), Cu-BPy@Am-SiO_2@Fe_3O_4 (30 mg), H_2O_2 (3 equiv), I_2 (1.2 equiv), DMF (3 mL), r.t. [b]Conversion percentages determined *via* GC-MS have been given in parentheses. [c]TON is the number of moles of the product per mole of the catalyst.

Scheme 4. Control Experiments for Probing Reaction Mechanism

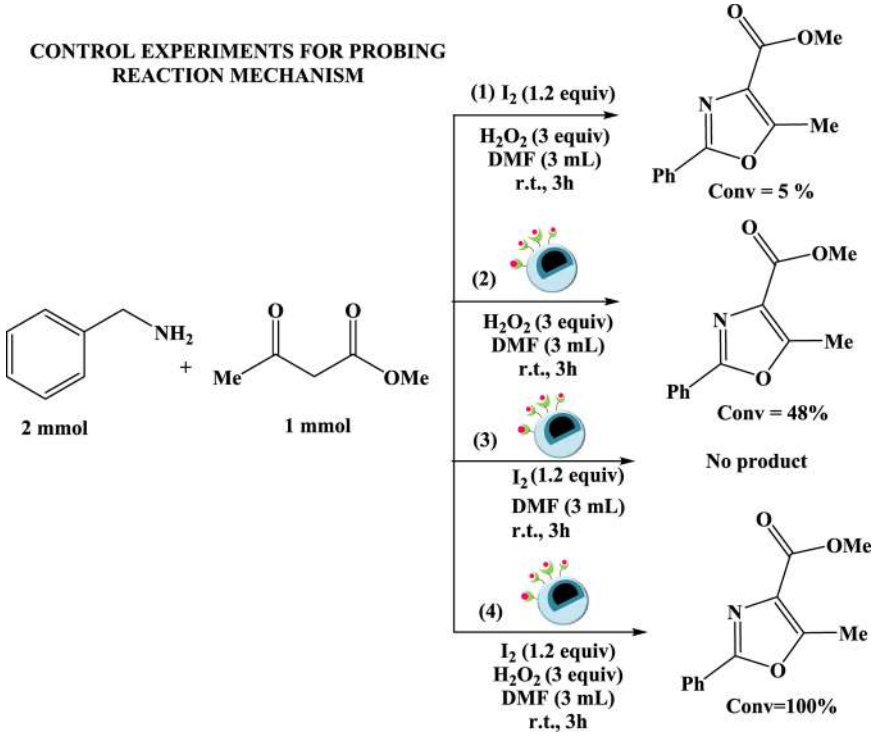

with ethanol, and dried under vacuum. It was observed that the catalyst could be reused at least eight times without any appreciable loss of activity. This observation was further supported by the SEM analysis of the recovered catalyst. The

DOI: 10.1021/acsomega.7b00382
ACS Omega 2017, 2, 2778–2791

Scheme 5. Proposed Mechanism for Cu-BPy@Am-SiO_2@Fe_3O_4-Catalyzed Tandem Oxidative Cyclization of Amines and 1,3-Dicarbonyls for the Synthesis of Polysubstituted Oxazoles

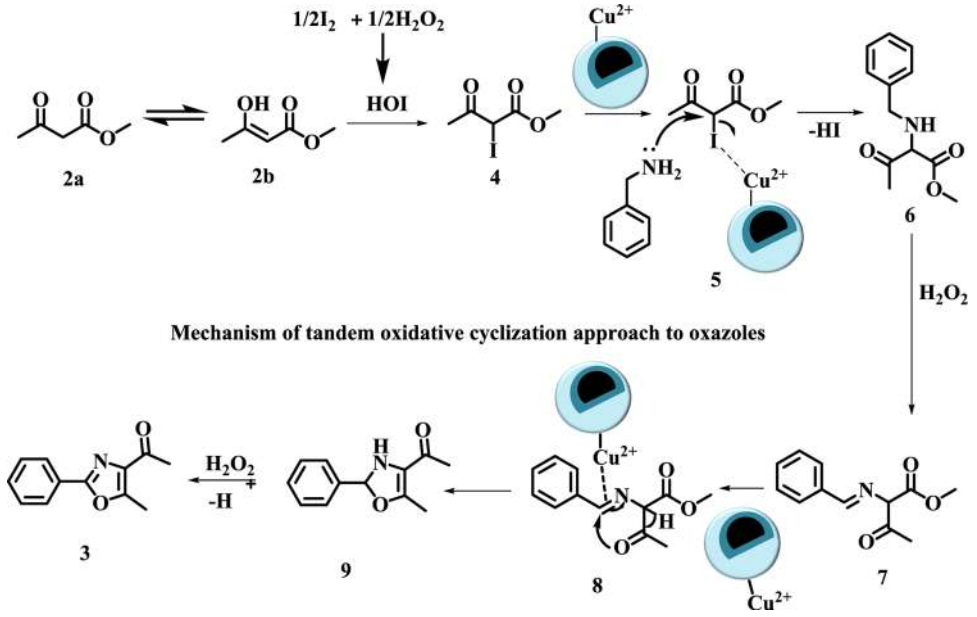

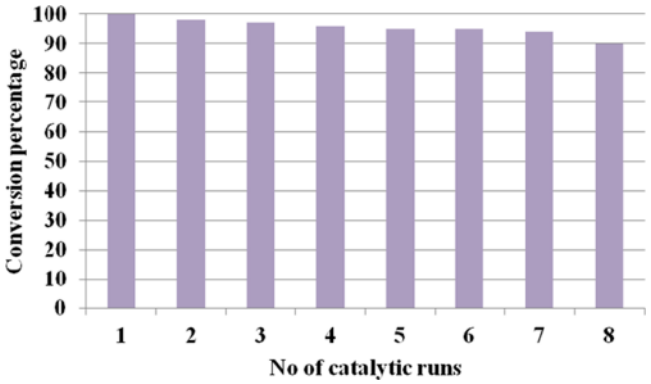

Figure 10. Recycling experiment for the tandem oxidative cyclization of amines and 1,3-dicarbonyls [reaction conditions: methylacetoacetate (1 mmol), benzylamine (2 mmol), Cu-BPy@Am-SiO_2@Fe_3O_4 catalyst (30 mg), H_2O_2 (3 equiv), I_2 (1.2 equiv), DMF (3 mL), r.t., 3 h].

SEM image of the recovered catalyst showed that the morphology of the synthesized Cu-BPy@Am-SiO_2@Fe_3O_4 nanoparticles remained intact, which provided a concrete proof of the excellent durability of the catalyst (Figure S3).

2.5. Comparison with Previous Studies. To shed light on the merit of the current protocol, a comparative analogy on the activities of the fabricated magnetite-supported copper nanocatalyst has been made with all of the previously reported methodologies for the tandem oxidative cyclization of amines and 1,3-dicarbonyls. Consequently, for drawing the best comparison, an in-depth analysis of crucial reaction parameters associated with the synthesis of industrially significant oxazoles has been carried out and factors such as reaction yield and conditions have been focused upon. A close introspection of the results clearly shows the superiority of our methodology (Table S2). The reactions yields are higher, and the conditions are also green (use of a green oxidant, H_2O_2). Besides, unlike other methods that employ homogeneous catalyst, our protocol uses a heterogeneous base metal nanocatalyst that is magnetically retrievable and hence can overcome the problems associated with catalyst separation and decomposition. Undoubtedly, it is the overall simplicity (no electrolysis conditions required unlike entries 3 and 4) and the economic competitiveness (owing to exceptional catalytic reusability) of this synthetic route that render it an appealing alternative to the literature precedents.

3. CONCLUSIONS

In the present study, we unveiled the fabrication of a new heterogeneous nanocatalyst possessing core−shell morphology for the synthesis of polysubstituted oxazoles obtained via the tandem oxidative cyclization approach. The catalyst is synthesized simply by the covalent immobilization of a copper−BPy complex on a silica-encapsulated magnetite nanosupport using inexpensive precursors under benign conditions. Sophisticated physicochemical tools, such as WAXRD, HRTEM, SEM, EDX, EDXRF, ICP, and FTIR analyses, have been employed for the structural confirmation of the synthesized organic−inorganic hybrid nanocatalyst. The efficacy of the synthesized Cu-BPy@Am-SiO_2@Fe_3O_4 catalyst can be realized by focusing on the results of various catalytic activity tests conducted, which include investigation of substrate scope, hot filtration, and recyclability experiments. This new methodology not only offers a convenient access to industrially significant oxazoles with promising yield, but it is also operationally facile and economically competitive compared with the literature precedents, as it employs a catalyst that is magnetically retrievable, reusable up to eight catalytic cycles, and highly durable. Besides, some of the other advantages include high atom economy, excellent turnover number, green reaction conditions (H_2O_2 as the oxidant), and applicability to gram-scale synthesis. As this study is based on the perfect combination of heterogeneous catalysis and tandem oxidative cyclization, it provides a distinct advancement toward the development of a sustainable approach for oxazole synthesis.

DOI: 10.1021/acsomega.7b00382
ACS Omega 2017, 2, 2778−2791

4. EXPERIMENTAL SECTION

4.1. Chemicals, Instrumentation, and Analysis. All chemicals, reagents, and solvents for the preparation of the catalyst and target compounds were of analytical grade, procured from commercial suppliers and used without further purification unless specified. In particular, TEOS (99.9%), APTES (98%), and BPy were purchased from Sigma-Aldrich, Fluka, and Alfa Aesar, respectively. Ultrapure Milli-Q water was used throughout for the preparation of all aqueous solutions. The entire oxidative cascade protocol was conducted under ambient atmospheric conditions. For analytical and preparative thin-layer chromatography (TLC), 0.2 mm (Merck) and 0.5 mm (Kieselgel GF254) precoated plates were used, respectively. The spots were visualized under UV light. In-depth characterization of the catalyst was carried out using different spectroscopic and microscopic techniques, such as FTIR, powder X-ray diffraction (PXRD), TEM, FESEM, EDX, VSM, EDXRF, X-ray photoelectron (XPS), and ICP analyses. FTIR spectra of the various stages of the nanocatalyst/obtained nanocomposites were recorded on a PerkinElmer Spectrum 2000 FTIR spectrometer (using the KBr pellet method) in the operating range of 4000−400 cm^{-1} under atmospheric conditions with a resolution of 1 cm^{-1}. PXRD patterns of the samples were collected with a Bruker D8 Advance (Karlsruhe, Bundesland, Germany) diffractometer using Cu/Kα radiation at a scanning rate of 4° min^{-1} in the 2θ range of 5−80° (λ = 0.15405 nm, 40 kV, 40 mA). The magnetization measurements of the bare and coated nanoparticles were performed at r.t. using a VSM (ADE-EV9; MicroSense) in an applied magnetic field sweeping from −22 000 to 22 000 Oe. Inductively coupled plasma mass spectrometry (ICP-MS) analysis was also accomplished to confirm the copper loading of the catalyst using ICP-MS (model no.: 7700e). To carry out the microwave-assisted digestion of the nanocatalyst, an Anton Paar Multiwave 3000 microwave instrument equipped with a temperature and pressure sensor was used. For studying the morphological characteristics (i.e., size, shape, and composition), microscopic techniques such as TEM and SEM were employed. The TEM images of the obtained nanocomposites were captured by a transmission electron microscope JEOL 2100F. The sample for TEM analysis was prepared by dispersing the nanoparticles in a high-purity ethanol solution under ultrasonic irradiation, followed by placing one drop of the suspended solution onto the TEM grid (copper grid coated with carbon film) before drying at r.t. under ambient conditions. On the other hand, a Tescan MIRA 3 FESEM instrument was employed for FESEM and EDX imaging of the samples. Finally, for investigating the percentage conversion, GC−MS analysis of all of the derived products was done using an Agilent gas chromatograph (6850 GC) with HP-5MS 5% phenyl methyl siloxane capillary column (30.0 m × 250 μm × 0.25 μm) and a quadrupole mass-filter-equipped 5975 mass-selective detector using helium as the carrier gas (rate: 0.9 mL min^{-1}).

4.2. Design and Synthesis of Nanocatalyst (Cu-BPy@Am-SiO_2@Fe_3O_4). *4.2.1. Synthesis of Amine-Functionalized Silica-Encapsulated Magnetite Nanosupport (Am-SiO_2@Fe_3O_4).* At the outset, magnetite nanoparticles were prepared via chemical coprecipitation of Fe(II) and Fe(III) salts in an ammoniacal medium.[67] In a typical procedure, 6.0 g of ferric sulfate and 4.2 g of ferrous sulfate were dissolved well in ultrapure water (250 mL) and stirred at 60 °C. A yellow-orange solution was obtained once the Fe (II) and Fe (III) salts dissolved completely in water. Thereafter, 15 mL of 25% NH_4OH was added dropwise into the reaction solution until the pH of the solution reached 10. The resulting solution was stirred continuously and vigorously for 1 h. The obtained black precipitate of Fe_3O_4 nanoparticles were separated using an external magnet, washed thoroughly with water and ethanol several times, and dried under vaccum. Next, the dried Fe_3O_4 nanoparticles were coated with silica using the modified sol−gel approach.[68] TEOS was used as the silica precursor for the coating process. This step was carried out by first dispersing Fe_3O_4 nanoparticles in ethanol under ultrasonic irradiation for 1 h. Subsequently, to the dispersed nanoparticles, 6 mL of ammonia and 2 mL of TEOS were added. This reaction mixture was stirred incessantly under atmospheric conditions for about 24 h. The synthesized SiO_2@Fe_3O_4 nanoparticles were isolated again using magnetic attraction, washed well with ethanol, and dried under vacuum. After the silica-coating process, amine groups were introduced onto the surface of the SiO_2@Fe_3O_4 nanoparticles using APTES as the functionalizing agent.[69] For this functionalization step, 5 mL of APTES was added to 1.0 g of SiO_2@Fe_3O_4 nanoparticles ultrasonically dispersed in 200 mL of ethanol solution and the resultant mixture was stirred for 24 h at r.t. The amine-functionalized nanocomposites (Am-SiO_2@Fe_3O_4) thus obtained were separated magnetically, washed many times with ethanol, and ultimately dried under vacuum.

4.2.2. Synthesis of the Nanocatalyst (Cu-BPy@Am-SiO_2@Fe_3O_4). The last stage of catalyst preparation involved two important steps: (1) covalent grafting of ligand and (2) metallation. The ligand-grafting process was carried out by refluxing 2 g of Am-SiO_2@Fe_3O_4 nanoparticles with BPy (4 mmol, 0.736 g) in ethanol for 10 h.[70] The ligand-grafted nanoparticles (BPy@Am-SiO_2@Fe_3O_4) so obtained were separated by magnetic attraction, washed well with ethanol at least three times to remove any unreacted ligand, and oven-dried for 10 h. Subsequently, 1.0 g of BPy@Am-SiO_2@Fe_3O_4 nanoparticles was reacted with 1.5 mmol of copper acetate for 6 h in absolute ethanol at r.t. for 24 h. The solvent was evaporated under vacuum, and the metallated nanoparticles were washed thoroughly with ethanol and dried in an oven for 2 h to obtain the final nanocatalyst (Scheme 1).

4.3. General Catalytic Procedure for the Synthesis of Polysubstituted Oxazoles via the Tandem Oxidative Cyclization Approach. To a reaction vessel containing benzylamine derivatives (2 mmol) in DMF (3 mL), iodine (1.2 equiv), 1,3-dicarbonyl compounds (1 mmol), catalyst (30 mg), and H_2O_2 (3 equiv) were added successively. The resulting reaction mixture was stirred at r.t. for an appropriate period of time, and the progress of the reaction was monitored via TLC. After the reaction, the catalyst was separated simply using an external bar magnet and the reaction contents were extracted with ethyl acetate. The organic layer was separated, dried over solid anhydrous sodium sulfate, and concentrated. Finally, the products were confirmed through the GC−MS technique.

■ ASSOCIATED CONTENT

Supporting Information

The Supporting Information is available free of charge on the ACS Publications website at DOI: 10.1021/acsomega.7b00382.

Additional material characterization data (PDF)

DOI: 10.1021/acsomega.7b00382
ACS Omega 2017, 2, 2778−2791

AUTHOR INFORMATION

Corresponding Author

*E-mail: rksharmagreenchem@hotmail.com. Tel: 011-276666250. Fax: +91-011-27666250.

ORCID

Rakesh K. Sharma: 0000-0003-4281-876X

Author Contributions

The manuscript was written through contributions of all authors. All authors have given approval to the final version of the manuscript.

Notes

The authors declare no competing financial interest.

ACKNOWLEDGMENTS

S.D. expresses her gratitude to University Grants Commission, Delhi, India, for awarding Senior Research Fellowship. The authors thank USIC-CLF, DU for FTIR, XRD, and VSM analyses and JNU for TEM analysis.

REFERENCES

(1) Grondal, C.; Jeanty, M.; Enders, D. Organocatalytic cascade reactions as a new tool in total synthesis. *Nat. Chem.* **2010**, *2*, 167−178.

(2) Nicolaou, K. C.; Edmonds, D. J.; Bulger, P. G. Cascade reactions in total synthesis. *Angew. Chem., Int. Ed.* **2006**, *45*, 7134−7186.

(3) Parsons, P. J.; Penkett, C. S.; Shell, A. J. Tandem reactions in organic synthesis: novel strategies for natural product elaboration and the development of new synthetic methodology. *Chem. Rev.* **1996**, *96*, 195−206.

(4) Nicolaou, K. C.; Montagnon, T.; Snyder, S. A. Tandem reactions, cascade sequences and biomimetic strategies in total synthesis. *Chem. Commun.* **2003**, *5*, 551−564.

(5) Behr, A.; Vorholt, A. J.; Ostrowski, K. A.; Seidensticker, T. Towards resource efficient chemistry: tandem reactions with renewables. *Green Chem.* **2014**, *16*, 982−1006.

(6) Ho, T. L. *Tandem organic reactions*; John Wiley & Sons, 1992.

(7) Medley, J. W.; Movassaghi, M. Robinson's landmark synthesis of tropinone. *Chem. Commun.* **2013**, *49*, 10775−10777.

(8) Li, C. J.; Trost, B. M. Green chemistry for chemical synthesis. *Proc. Natl. Acad. Sci. U.S.A.* **2008**, *105*, 13197−13202.

(9) McCarroll, A. J.; Walton, J. C. Organic syntheses through free-radical annulations and related cascade sequences. *J. Chem. Soc., Perkin Trans. 1* **2001**, *24*, 3215−3229.

(10) Naresh, G.; Narender, T. Molecular iodine mediated synthesis of polysubstituted oxazoles by oxidative domino cyclization in water. *RSC Adv.* **2014**, *4*, 11862−11866.

(11) Wan, C.; Hang, J.; Wang, S.; Fan, J.; Wang, Z. Facile synthesis of polysubstituted oxazoles via a copper-catalyzed tandem oxidative cyclization. *Org. Lett.* **2010**, *12*, 2338−2341.

(12) Jiang, H.; Huang, H.; Cao, H.; Qi, C. TBHP/I_2-mediated domino oxidative cyclization for one-pot synthesis of polysubstituted oxazoles. *Org. Lett.* **2010**, *12*, 5561−5563.

(13) Zheng, M.; Huang, L.; Huang, H.; Li, X.; Wu, W.; Jiang, H. Palladium-Catalyzed Sequential C−N/C−O Bond Formations: Synthesis of Oxazole Derivatives from Amides and Ketones. *Org. Lett.* **2014**, *16*, 5906−5909.

(14) Yuan, G.; Zhu, Z.; Gao, X.; Jiang, H. Electrochemically promoted synthesis of polysubstituted oxazoles from β-diketone derivatives and benzylamines under mild conditions. *RSC Adv.* **2014**, *4*, 24300−24303.

(15) Hu, P.; Wang, Q.; Yan, Y.; Zhang, S.; Zhang, B.; Wang, Z. CuI-catalyzed and air promoted oxidative cyclization for one-pot synthesis of polyarylated oxazoles. *Org. Biomol. Chem.* **2013**, *11*, 4304−4307.

(16) Chng, L. L.; Erathodiyil, N.; Ying, J. Y. Nanostructured catalysts for organic transformations. *Acc. Chem. Res.* **2013**, *46*, 1825−1837.

(17) Philippot, K.; Serp, P. Concepts in nanocatalysis. In *Nanomaterials in Catalysis*, 1st ed.; Wiley-VCH Verlag GmbH, 2013; pp 1−54.

(18) Mondal, J.; Biswas, A.; Chiba, S.; Zhao, Y. Cu^0 nanoparticles deposited on nanoporous polymers: a recyclable heterogeneous nanocatalyst for Ullmann coupling of aryl halides with amines in water. *Sci. Rep.* **2015**, *5*, No. 8294.

(19) Collis, A. E.; Horvath, I. T. Heterogenization of homogeneous catalytic systems. *Catal. Sci. Technol.* **2011**, *1*, 912−919.

(20) Narani, A.; Marella, R. K.; Ramudu, P.; Rao, K. S. R.; Burri, D. R. Cu (II) complex heterogenized on SBA-15: a highly efficient and additive-free solid catalyst for the homocoupling of alkynes. *RSC Adv.* **2014**, *4*, 3718−3725.

(21) Ogasawara, S.; Kato, S. Palladium nanoparticles captured in microporous polymers: a tailor-made catalyst for heterogeneous carbon cross-coupling reactions. *J. Am. Chem. Soc.* **2010**, *132*, 4608−4613.

(22) Veisi, H.; Hamelian, M.; Hemmati, S. Palladium anchored to SBA-15 functionalized with melamine-pyridine groups as a novel and efficient heterogeneous nanocatalyst for Suzuki−Miyaura coupling reactions. *J. Mol. Catal. A: Chem.* **2014**, *395*, 25−33.

(23) Schätz, A.; Reiser, O.; Stark, W. J. Nanoparticles as Semi-Heterogeneous Catalyst Supports. *Chem. − Eur. J.* **2010**, *16*, 8950−8967.

(24) Panigrahi, S.; Basu, S.; Praharaj, S.; Pande, S.; Jana, S.; Pal, A.; et al. Synthesis and size-selective catalysis by supported gold nanoparticles: study on heterogeneous and homogeneous catalytic process. *J. Phys. Chem. C.* **2007**, *111*, 4596−4605.

(25) Wang, Y.; Xiao, Z.; Wu, L. Metal-nanoparticles supported on solid as heterogeneous catalysts. *Curr. Org. Chem.* **2013**, *17*, 1325−1333.

(26) El-Shall, M. S.; Abdelsayed, V.; Abd El Rahman, S. K.; Hassan, H. M.; El-Kaderi, H. M.; Reich, T. E. Metallic and bimetallic nanocatalysts incorporated into highly porous coordination polymer MIL-101. *J. Mater. Chem.* **2009**, *19*, 7625−7631.

(27) Stiles, A. B. *Catalyst supports and supported catalysts*; Butterworth Publishers: Stoneham, 1987.

(28) Julkapli, N. M.; Bagheri, S. Graphene supported heterogeneous catalysts: an overview. *Int. J. Hydrogen Energy* **2015**, *40*, 948−979.

(29) Dang, T. T.; Zhu, Y.; Ngiam, J. S.; Ghosh, S. C.; Chen, A.; Seayad, A. M. Palladium nanoparticles supported on ZIF-8 as an efficient heterogeneous catalyst for aminocarbonylation. *ACS Catal.* **2013**, *3*, 1406−1410.

(30) Xie, W.; Hu, L.; Yang, X. Basic ionic liquid supported on mesoporous SBA-15 silica as an efficient heterogeneous catalyst for biodiesel production. *Ind. Eng. Chem. Res.* **2015**, *54*, 1505−1512.

(31) Shang, L.; Bian, T.; Zhang, B.; Zhang, D.; Wu, L. Z.; Tung, C. H.; Zhang, T.; et al. Graphene-supported ultrafine metal nanoparticles encapsulated by mesoporous silica: robust catalysts for oxidation and reduction reactions. *Angew. Chem., Int. Ed.* **2014**, *53*, 250−254.

(32) Gallon, B. J.; Kojima, R. W.; Kaner, R. B.; Diaconescu, P. L. Palladium Nanoparticles Supported on Polyaniline Nanofibers as a Semi-Heterogeneous Catalyst in Water. *Angew. Chem., Int. Ed.* **2007**, *46*, 7251−7254.

(33) Xie, W.; Li, H. Alumina-supported potassium iodide as a heterogeneous catalyst for biodiesel production from soybean oil. *J. Mol. Catal. A: Chem.* **2006**, *255*, 1−9.

(34) Ballini, R.; Bosica, G.; Fiorini, D.; Maggi, R.; Righi, P.; Sartori, G.; Sartorio, R. MCM-41-TBD as a new, efficient, supported heterogeneous catalyst for the synthesis of thioureas. *Tetrahedron Lett.* **2002**, *43*, 8445−8447.

(35) Zhu, A.; Jiang, T.; Han, B.; Zhang, J.; Xie, Y.; Ma, X. Supported choline chloride/urea as a heterogeneous catalyst for chemical fixation of carbon dioxide to cyclic carbonates. *Green Chem.* **2007**, *9*, 169−172.

(36) Mori, K.; Hara, T.; Mizugaki, T.; Ebitani, K.; Kaneda, K. Hydroxyapatite-supported palladium nanoclusters: a highly active heterogeneous catalyst for selective oxidation of alcohols by use of molecular oxygen. *J. Am. Chem. Soc.* **2004**, *126*, 10657−10666.

(37) Liu, H.; Liu, Y.; Li, Y.; Tang, Z.; Jiang, H. Metal− organic framework supported gold nanoparticles as a highly active

DOI: 10.1021/acsomega.7b00382
ACS Omega 2017, 2, 2778−2791

heterogeneous catalyst for aerobic oxidation of alcohols. *J. Phys. Chem. C* **2010**, *114*, 13362−13369.
(38) Zhang, Q.; Luo, J.; Wei, Y. A silica gel supported dual acidic ionic liquid: an efficient and recyclable heterogeneous catalyst for the one-pot synthesis of amidoalkyl naphthols. *Green Chem.* **2010**, *12*, 2246−2254.
(39) Ahmed, N.; Siddiqui, Z. N. Cerium Supported Chitosan as an Efficient and Recyclable Heterogeneous Catalyst for Sustainable Synthesis of Spiropiperidine Derivatives. *ACS Sustainable Chem. Eng.* **2015**, *3*, 1701−1707.
(40) Gawande, M. B.; Monga, Y.; Zboril, R.; Sharma, R. K. Silica-decorated magnetic nanocomposites for catalytic applications. *Coord. Chem. Rev.* **2015**, *288*, 118−143.
(41) Sharma, R. K.; Dutta, S.; Sharma, S.; Zboril, R.; Varma, R. S.; Gawande, M. B. Fe_3O_4 (iron oxide)-supported nanocatalysts: synthesis, characterization and applications in coupling reactions. *Green Chem.* **2016**, *18*, 3184−3209.
(42) Sharma, R. K.; Yadav, M.; Gawande, M. B. Silica-Coated Magnetic Nano-Particles: Application in Catalysis. *ACS Symp. Ser.* **2016**, *1238*, 1−38.
(43) Lu, A. H.; Salabas, E. E.; Schüth, F. Magnetic nanoparticles: synthesis, protection, functionalization, and application. *Angew. Chem., Int. Ed.* **2007**, *46*, 1222−1244.
(44) Rossi, L. M.; Costa, N. J.; Silva, F. P.; Wojcieszak, R. Magnetic nanomaterials in catalysis: advanced catalysts for magnetic separation and beyond. *Green Chem.* **2014**, *16*, 2906−2933.
(45) Shylesh, S.; Schünemann, V.; Thiel, W. R. Magnetically separable nanocatalysts: bridges between homogeneous and heterogeneous catalysis. *Angew. Chem., Int. Ed.* **2010**, *49*, 3428−3459.
(46) Varma, R. S.; Verma, S.; Nadagouda, M. N.; Baig, R. N. Advancing Sustainable Catalysis with Magnetite. Surface Modification and Synthetic Applications. *Aldrichim. Acta* **2016**, *49*, 35−41.
(47) Laurent, S.; Forge, D.; Port, M.; Roch, A.; Robic, C.; Vander, E. L.; Muller, R. N. Magnetic iron oxide nanoparticles: synthesis, stabilization, vectorization, physicochemical characterizations, and biological applications. *Chem. Rev.* **2008**, *108*, 2064−2110.
(48) Yu, L.; Wang, M.; Li, P.; Wang, L. Fe_3O_4 nanoparticle-supported copper (I): magnetically recoverable and reusable catalyst for the synthesis of quinazolinones and bicyclic pyrimidinones. *Appl. Organomet. Chem.* **2012**, *26*, 576−582.
(49) Le, X.; Dong, Z.; Jin, Z.; Wang, Q.; Ma, J. Suzuki−Miyaura cross-coupling reactions catalyzed by efficient and recyclable Fe_3O_4@SiO_2@mSiO_2−Pd (II) catalyst. *Catal. Commun.* **2014**, *53*, 47−52.
(50) Zhang, L.; Li, P.; Liu, C.; Yang, J.; Wang, M.; Wang, L. A highly efficient and recyclable Fe_3O_4 magnetic nanoparticle immobilized palladium catalyst for the direct C-2 arylation of indoles with arylboronic acids. *Catal. Sci. Techol.* **2014**, *4*, 1979−1988.
(51) Zolfigol, M. A.; Khakyzadeh, V.; Moosavi-Zare, A. R.; Rostami, A.; Zare, A.; Iranpoor, N.; et al. A highly stable and active magnetically separable Pd nanocatalyst in aqueous phase heterogeneously catalyzed couplings. Luque, R. *Green Chem.* **2013**, *15*, 2132−2140.
(52) Ying, A.; Hou, H.; Liu, S.; Chen, G.; Yang, J.; Xu, S. Ionic Modified TBD Supported on Magnetic Nanoparticles: A Highly Efficient and Recoverable Catalyst for Organic Transformations. *ACS Sustainable Chem. Eng.* **2016**, *4*, 625−632.
(53) Liu, Y. H.; Deng, J.; Gao, J. W.; Zhang, Z. H. Triflic Acid-Functionalized Silica-Coated Magnetic Nanoparticles as a Magnetically Separable Catalyst for Synthesis of gem-Dihydroperoxides. *Adv. Synth. Catal.* **2012**, *354*, 441−447.
(54) Sharma, R. K.; Dutta, S.; Sharma, S. Quinoline-2-carboimine copper complex immobilized on amine functionalized silica coated magnetite nanoparticles: a novel and magnetically retrievable catalyst for the synthesis of carbamates via C−H activation of formamides. *Dalton Trans.* **2015**, *44*, 1303−1316.
(55) Sharma, R. K.; Dutta, S.; Sharma, S. Nickel (ii) complex covalently anchored on core shell structured SiO_2@Fe_3O_4 nanoparticles: a robust and magnetically retrievable catalyst for direct one-pot reductive amination of ketones. *New J. Chem.* **2016**, *40*, 2089−2101.
(56) Sharma, R. K.; Sharma, S.; Dutta, S.; Zboril, R.; Gawande, M. B. Silica-nanosphere-based organic−inorganic hybrid nanomaterials: synthesis, functionalization and applications in catalysis. *Green Chem.* **2015**, *17*, 3207−3230.
(57) Sharma, R. K.; Yadav, M.; Monga, Y.; Gaur, R.; Adholeya, A.; Zboril, R.; Gawande, M. B.; et al. Silica-based Magnetic Manganese Nanocatalyst−Applications in the Oxidation of Organic Halides and Alcohols. *ACS Sustainable Chem. Eng.* **2016**, *4*, 1123−1130.
(58) Sharma, R. K.; Gaur, R.; Yadav, M.; Rathi, A. K.; Pechousek, J.; Petr, M.; Gawande, M. B.; et al. Maghemite-Copper Nanocomposites: Applications for Ligand-Free Cross-Coupling (C− O, C− S, and C− N) Reactions. *ChemCatChem* **2015**, *7*, 3495−3502.
(59) Sharma, R. K.; Yadav, M.; Gaur, R.; Monga, Y.; Adholeya, A. Magnetically retrievable silica-based nickel nanocatalyst for Suzuki−Miyaura cross-coupling reaction. *Catal. Sci. Technol.* **2015**, *5*, 2728−2740.
(60) Sharma, R. K.; Monga, Y.; Puri, A.; Gaba, G. Magnetite (Fe_3O_4) silica based organic−inorganic hybrid copper (ii) nanocatalyst: a platform for aerobic N-alkylation of amines. *Green Chem.* **2013**, *15*, 2800−2809.
(61) Sharma, R. K.; Monga, Y.; Puri, A. Magnetically separable silica@ Fe_3O_4 core−shell supported nano-structured copper (II) composites as a versatile catalyst for the reduction of nitroarenes in aqueous medium at room temperature. *J. Mol. Catal. A: Chem.* **2014**, *393*, 84−95.
(62) Sharma, R. K.; Monga, Y.; Puri, A. Zirconium (IV)-modified silica@magnetic nanocomposites: fabrication, characterization and application as efficient, selective and reusable nanocatalysts for Friedel−Crafts, Knoevenagel and Pechmann condensation reactions. *Catal. Commun.* **2013**, *35*, 110−114.
(63) Sharma, R. K.; Monga, Y. Silica encapsulated magnetic nanoparticles-supported Zn (II) nanocatalyst: A versatile integration of excellent reactivity and selectivity for the synthesis of azoxyarenes, combined with facile catalyst recovery and recyclability. *Appl. Catal., A* **2013**, *454*, 1−10.
(64) Sharma, R. K.; Sharma, S.; Gaba, G.; Dutta, S. Coordinated copper (II) supported on silica nanospheres applied to the synthesis of α-ketoamides via oxidative amidation of methyl ketones. *J. Mater. Sci.* **2016**, *51*, 2121−2133.
(65) Sharma, R. K.; Mishra, M.; Sharma, S.; Dutta, S. Zinc (II) complex immobilized on amine functionalized silica gel: a novel, highly efficient and recyclable catalyst for multicomponent click synthesis of 1, 4-disubstituted 1, 2, 3-triazoles. *J. Coord. Chem.* **2016**, *69*, 1152−1165.
(66) Sharma, R. K.; Pandey, A.; Gulati, S. Silica-supported palladium complex: An efficient, highly selective and reusable organic−inorganic hybrid catalyst for the synthesis of E-stilbenes. *Appl. Catal., A* **2012**, *431−432*, 33−41.
(67) Polshettiwar, V.; Baruwati, B.; Varma, R. S. Nanoparticle-supported and magnetically recoverable nickel catalyst: a robust and economic hydrogenation and transfer hydrogenation protocol. *Green Chem.* **2009**, *11*, 127−131.
(68) Zhang, Q.; Su, H.; Luo, J.; Wei, Y. A magnetic nanoparticle supported dual acidic ionic liquid: a "quasi-homogeneous" catalyst for the one-pot synthesis of benzoxanthenes. *Green Chem.* **2012**, *14*, 201−208.
(69) Pereira, C.; Pereira, A. M.; Quaresma, P.; Tavares, P. B.; Pereira, E.; Araújo, J. P.; Freire, C. Superparamagnetic γ-Fe_2O_3@SiO_2 nanoparticles: a novel support for the immobilization of [VO $(acac)_2$]. *Dalton Trans.* **2010**, *39*, 2842−2854.
(70) Karimi, B.; Zamani, A.; Abedi, S.; Clark, J. H. Aerobic oxidation of alcohols using various types of immobilized palladium catalyst: the synergistic role of functionalized ligands, morphology of support, and solvent in generating and stabilizing nanoparticles. *Green Chem.* **2009**, *11*, 109−119.
(71) Petcharoen, K.; Sirivat, A. Synthesis and characterization of magnetite nanoparticles via the chemical co-precipitation method. *Mater. Sci. Eng., B.* **2012**, *177*, 421−427.

DOI: 10.1021/acsomega.7b00382
ACS Omega 2017, 2, 2778−2791

(72) Wang, S.; Zhang, Z.; Liu, B.; Li, J. Silica coated magnetic Fe_3O_4 nanoparticles supported phosphotungstic acid: a novel environmentally friendly catalyst for the synthesis of 5-ethoxymethylfurfural from 5-hydroxymethylfurfural and fructose. *Catal. Sci. Technol.* **2013**, *3*, 2104−2112.
(73) Esmaeilpour, M.; Sardarian, A. R.; Javidi, J. Synthesis and characterization of Schiff base complex of Pd (II) supported on superparamagnetic Fe_3O_4@SiO_2 nanoparticles and its application as an efficient copper-and phosphine ligand-free recyclable catalyst for Sonogashira−Hagihara coupling reactions. *J. Organomet. Chem.* **2014**, *749*, 233−240.
(74) Martín, R.; Cuenca, A.; Buchwald, S. L. Sequential copper-catalyzed vinylation/cyclization: An efficient synthesis of functionalized oxazoles. *Org. Lett.* **2007**, *9*, 5521−5524.
(75) Wan, J. P.; Lin, Y.; Cao, X.; Liu, Y.; Wei, L. Correction: Copper-catalyzed, hypervalent iodine mediated C [double bond, length as m-dash] C bond activation of enaminones for the synthesis of α-keto amides. *Chem. Commun.* **2016**, *52*, 4393.
(76) Gawande, S. D.; Kavala, V.; Zanwar, M. R.; Kuo, C. W.; Huang, H. N.; He, C. H.; Yao, C. F.; et al. Molecular Iodine-Mediated Cascade Reaction of 2-Alkynylbenzaldehyde and Indole: An Easy Access to Tetracyclic Indoloazulene Derivatives. *Adv. Synth. Catal.* **2013**, *355*, 3022−3036.
(77) Xie, Y. X.; Yan, Z. Y.; Qian, B.; Deng, W. Y.; Wang, D. Z.; Wu, L. Y.; Liang, Y. M.; et al. A novel iodine-mediated tandem cyclization−cycloaddition reaction leading to polyoxacyclic ring systems. *Chem. Commun.* **2009**, *36*, 5451−5453.
(78) Akbar, S.; Srinivasan, K. Iron (III) halide or iodine-promoted synthesis of 3-haloindene derivatives from o-alkynylarene chalcones. *RSC Adv.* **2015**, *5*, 5542−5545.
(79) Nakatake, D.; Yazaki, R.; Matsushima, Y.; Ohshima, T. Transesterification Reactions Catalyzed by a Recyclable Heterogeneous Zinc/Imidazole Catalyst. *Adv. Synth. Catal.* **2016**, *358*, 2569−2574.

DOI: 10.1021/acsomega.7b00382
ACS Omega 2017, 2, 2778−2791